# Imaging 2D Breast Cancer Tumor Margin at Terahertz Frequency using Numerical Field Data based on DDSCAT

**T. C. Bowman, A. M. Hassan, and M. El-Shenawee**

Department of Electrical Engineering
University of Arkansas, Fayetteville, AR 72701, USA
tcbowman@uark.edu, amhassan@uark.edu, magda@uark.edu

***Abstract*** ― This work presents tomography of breast cancer tumor margins in the terahertz frequency band. The discrete dipole approximation is employed to calculate the electromagnetic fields scattered from simulated heterogeneous breast tumors. Two-dimensional Comedo with necrotic core and papillary breast tumor patterns are computer-generated for this investigation. The Rytov approximation is applied to terahertz scattered field data calculated at a line of receivers in the far field from the samples. The obtained tomography images demonstrate a potential for terahertz frequency for identifying and assessment of breast cancer tumor margins.

***Index Terms*** – Breast cancer, discrete dipole approximation (DDSCAT), Rytov tomography, and terahertz imaging.

## I. INTRODUCTION

In the conservative treatment of sufficiently small breast tumors, lumpectomy is the preferred procedure for excising cancerous tissues. In this treatment, the tumor is removed via surgery in addition to a few millimeters of healthy tissue surrounding the tumor. The margins of this removed tumor are examined by pathologists via histo-pathological analysis and classified into one of three types. A *positive* margin indicates that cancerous tissue exceeds the edge of the healthy margin; a *negative* margin indicates that there is no cancerous tissue within 1-2mm of the edge; and a *close* margin indicates that the cancerous tissue lies less than 1 mm of the margin boundary but does not exceed it. In the case of a positive or close margin identified in the excised tissue, a second surgery is required to remove the remaining cancerous tissues.

However, pathology analysis of these margins generally requires several days in order to be processed fully, meaning that any secondary procedure will require the patient to return at a later date. Furthermore, it is reported in [1] that up to 20-70 % of the time, pathology reports indicate the presence of positive margins following the lumpectomy. It is also mentioned that the need for a second surgery at a later date increases the risk of patient breast disfigurement, increases the resource burden on the patient, and decreases patient morale and confidence in the surgeon [1].

As reported in [2], an ideal technique for improving cancer margin assessment would be able to analyze the excision intra-operatively with a sensing depth of at least 1-2 mm. It would furthermore need to provide a 3D image of the tumor surface that is easily read by a surgeon in the operating room. The developed technique would need to be accurate enough to reduce repeated surgery rates by allowing surgeons to detect and remove cancerous tissue within the same procedure as the lumpectomy.

Recently, the terahertz (THz) frequency range has been suggested as a potential tool in the use of cancer detection and classification [3-5]. THz imaging is attractive for its ability to penetrate materials to a depth of several millimeters, giving it an advantage over optical techniques in addressing the concerns reported in [2]. Terahertz waves also lack the polarization energy of x-rays, making them more attractive for *in vivo* applications, as well as having a higher resolution than microwave imaging. The THz range from 0.01 THz to 2 THz has been shown to be

*Submitted On: May 29, 2013*
*Accepted On: Oct. 14, 2013*

particularly useful for cancer detection due to noticeable differences in electrical properties between cancerous and healthy tissue in tumors taken from the breast and colon [3-5]. The assertion of inherent contrast of cancerous cells at high frequency has also been suggested in model-based photonics for the early detection of breast cancer [6]. However, the focus of this work is the use of a numerical THz model based on the discrete dipole approximation (DDSCAT). Additionally, the model is not for detecting breast tumors but for investigating the scattering from excised cancerous tissue in the terahertz band.

The authors of this work conducted preliminary experimental THz measurements from very few excised breast tissue samples fixed in formalin and embedded in paraffin (FFPE) [7]. The experimental THz imaging measurement reported in [7] was based on the directly reflected electric field from flat tissue samples. While the reported THz images in [7] were not adequate to assess tumor margins or cancer regions, the conclusions motivated the authors to first conduct modeling and simulation of the problem before proceeding further with the experimental work. An abstract of the current work has been previously presented in conferences [8, 9].

The goal of this paper is to simulate the tomography problem of cancer margins in order to understand the strengths and limitations, if any, of THz techniques for this application. The idea is to employ a modeling technique to calculate scattered electric fields from excised breast tumor samples using the setup diagramed in Fig. 1 and to implement a computer tomography method to reconstruct the cancer margins. This work adopts the DDSDCAT that has proven capability for calculating the scattered electric and magnetic fields from heterogeneous two- and three-dimensional objects [10-14]. To reconstruct the image of tumor margins, the well-known Rytov tomography algorithms will be applied to the synthetic simulated data [15-19]. Section II discusses the modeling methods and section III presents the numerical results. Conclusion and future work are presented in the section IV.

## II. METHODOLOGY

### A. Tumor model

In this work, the tumor patterns are generated using a multiple-nutrients tumor growth model developed by Ferreira *et al.* [20]. In the model, two nutrients are employed: (*i*) nutrient *M* necessary for survival of the cancerous cells and (*ii*) nutrient *N* necessary for the division of the cancerous cells. The utilization of two nutrients provides extra degrees of freedom that can be used to generate a wide variety of histologically accurate tumor patterns. The model is based on the diffusion of the nutrients *M* and *N* and the consumption of these nutrients by cancerous and healthy cells [20]. Healthy cells consume both nutrients *N* and *M* at a rate of $\alpha$ normalized values per unit time whereas cancerous cells consume nutrient *N* at a rate of $\lambda_N \times \alpha$ and consume nutrient *M* at a rate of $\lambda_M \times \alpha$. The parameters $\lambda_N$ and $\lambda_M$ are assumed larger than unity to account for the elevated consumption of nutrients by cancer cells. At each time step, the values of the nutrients *N* and *M* are updated according to their diffusion and consumption by cancer and healthy cells.

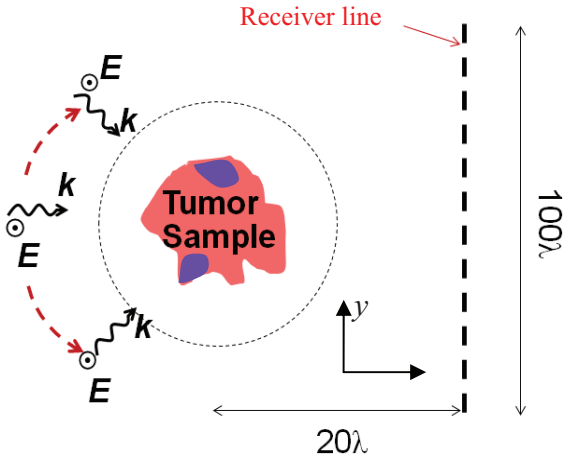


Fig. 1. 2D computational configuration of tumor sample, incident plane waves, and receiver line.

In addition, two cellular activities are implemented: (*i*) cell division and (*ii*) cell death. The probability of a cell dividing at a certain pixel is expressed as a function of the nutrient *N* at that pixel. The probability of a cell dying at a certain pixel is expressed as a function of the nutrient *M* at that pixel [20]. By varying the parameters $\alpha$, $\lambda_N$, and $\lambda_M$, different tumor patterns can be generated [21]. The particular tumor patterns developed and used in this paper are the Comedo pattern with a central necrotic core and the papillary pattern, as shown in Fig. 2 [21]. Each black square in the figure represents a cancer cell. These tumor

patterns were generated using a square computational domain of size 60×60 pixels [21]. The parameters used to generate the Comedo pattern in Fig. 2 (a) are ($\alpha$ = 0.032, $\lambda_N$ = 220, $\lambda_M$ = 220), and the parameters used to generate the papillary pattern in Fig. 2 (b) are ($\alpha$ = 0.05, $\lambda_N$ = 250, $\lambda_M$ = 20). More details about the model implementation and parameters are found in [20-21].

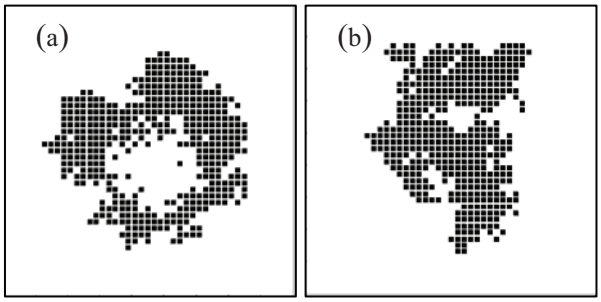


Fig. 2. (a) Comedo tumor pattern with necrotic core and (b) Papillary tumor pattern [21].

**B. Discrete dipole approximation (DDSCAT)**

For simplicity, in this work a two dimensional (2D) forward model will be implemented using the open source DDSCAT computer code available in serial or in MPI accelerated computer codes [13, 14]. The DDSCAT method is used for calculating the scattered electric fields from a simulated heterogeneous breast sample tissue as demonstrated in Fig. 1. This model is very desirable to simulate objects made of dispersive materials where the target under test is discretized into smaller particles, i.e., dipoles, of size very small compared with the wavelength. Examples of this discretization are shown in Fig. 3.

Each dipole in Fig. 3 can be made of a different anisotropic material. Therefore, the DDSCAT has the advantage of modeling highly heterogeneous targets, which presents a realistic method to model breast cancer tumor tissue. While there are other forward solvers to handle heterogeneous objects such as the finite difference time domain and finite element, among others, the DDSCAT requires that only the target be discretized and not the whole domain, making it attractive from the perspective of CPU time and memory requirements. The accuracy of the DDSCAT was numerically compared with four known methods: the Mie theory, the T-matrix method, the finite element method (ANSOFT HFSS), and the finite difference time domain (numerical FDTD solutions version 5.0) [22].

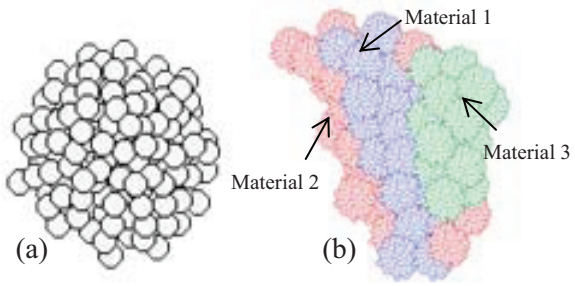


Fig. 3. (a) Sketch of a homogeneous object discretized into particles (i.e., dipoles) and (b) heterogeneous medium of irregular boundaries discretized into dipoles (reproduced) [11].

The dipoles of the discretized object in Fig. 3 acquire dipole moments in response to a local electric field. The method converges when $|n|\, kd < 0.5$, where $k$ is the wavenumber, $d$ is the dipole size, and $n$ is the complex index of refraction [10-14]. The method solves for the dipole moments at all dipole positions. The main equation of the open source code and additional details are given in appendix A and in references [10-14].

**C. Linearized inverse scattering technique**

The well-known Rytov algorithm approximates the nonlinear inverse scattering problem as a linear problem [15-19]. Thus the relation of the scattered field phase to the function of the object shape becomes linear. The refractive index of the unknown object is then obtained using the filtered back propagation (FBP) scheme. While Rytov linearized tomography method has the limitation of low contrast between the target and background, it offers implementation simplicity and good results in THz applications [23].

In Rytov approximation, the assumption is that the phase of the scattering field has small variations over a single wavelength. As the result, a linear relationship is assumed between the phase of the scattered field and the target object [16-18]. The relationship between the phase of the scattered and incident fields is expressed as follows [16-18, 24],

$$\psi_s(\bar{r}) = \frac{1}{\psi_{inc}(\bar{r})} \int_V G(\bar{r} - \bar{r}')\, \psi_{inc}(\bar{r}')\, O(\bar{r}')\, d\bar{r}' \quad (1)$$

where $\psi_s(\bar{r})$ represents the phase of scattered fields and $\psi_{inc}(\bar{r})$ represents the phase of the incident fields, $\bar{r}$ and $\bar{r}'$ represent the position vectors of the observation and source, respectively, $V$ is the computational volume, $G(\bar{r}-\bar{r}')$ is the dyadic Green's function, and $O(\bar{r}')$ is the profile of the unknown object to be reconstructed. The Fourier diffraction theorem is employed to reconstruct the profile of the unknown object. There are two possible methods to produce final results: the direct Fourier interpolation (DFI) and the filtered back propagation (FBP) algorithm. The difference between these methods lies in the way that the Fourier transform of the scattered-field data is interpolated. It is proven in [19] that the FBP method produces more reliable results and avoids some artifacts associated with the interpolation in the spatial frequency domain [19].

The Rytov algorithm requires the availability of the scattered fields from multiple incident directions, where the phase of these fields are as shown used in equation (1). In DDSCAT the excitation is a plane wave propagating in the positive $x$-direction (see Fig. 4). To achieve these multiple incident directions in DDSCAT, the target is rotated around the $z$-axis, which is effectively equivalent to rotating the incident directions. Thirty six equally-spaced orientations of the target around its axis are simulated. In each simulation, the fields scattered from the target are calculated. Since the simulation at each orientation is completely independent from the other orientations, an MPI code was developed to call 36 instances of DDSCAT, one for each orientation, in parallel on the STAR of Arkansas supercomputer. This reduces the computational time significantly to 1/36 of the value that would have been necessary if the orientations were run sequentially. Once the unknown index of refraction of the tissue is obtained using equation (1) at each pixel of the domain of Fig. 1, the image is reconstructed. More details can be found in [15-19].

## III. NUMERICAL RESULTS

All examples in this Section are modeled at frequency $f$ =1 THz ($\lambda$ = 300 μm) with 36 incident plane waves at angles evenly distributed around the 2D tumor sample shown in Fig. 1. The scattered electric fields are calculated on a line of 36 receivers of 100 λ long and at a distance of 20 λ from the center of the simulation domain as shown in Fig. 1.

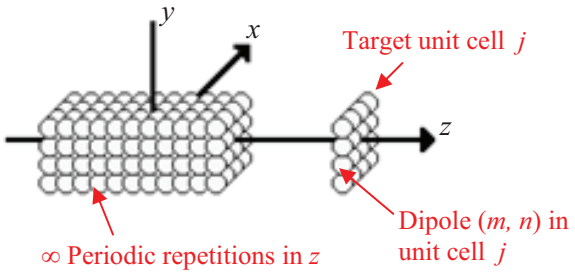


Fig. 4. DDSCAT model of infinite cylinder (reproduced) [11].

Figure 5 shows the DDSCAT model of the Comedo tumor pattern given in Fig. 1 (a). At 1 THz, cancerous tissue has $\varepsilon_r$ = 4 and fibrous tissue has $\varepsilon_r$ = 3.6. However, in this setup the cancerous tissue is assumed to have $\varepsilon_r$ = 1.133 and the surrounding fibrous (i.e., fibroglandular) tissue background $\varepsilon_r$ = 1.03. These values were selected such that the relative contrast between cancer and fibrous tissue is retained as 1.133/1.03 = 1.1 compared to 4/3.6 = 1.1 using the actual permittivity values. The lower permittivity values in this model are necessary for the use of Rytov approximation to find the contrast from the scattered field [15], since reconstructing the properties of the cancerous tissue relative to the fibrous background is the main interest of this work. The spacing of the dipoles is set to 0.04 λ at 1 THz.

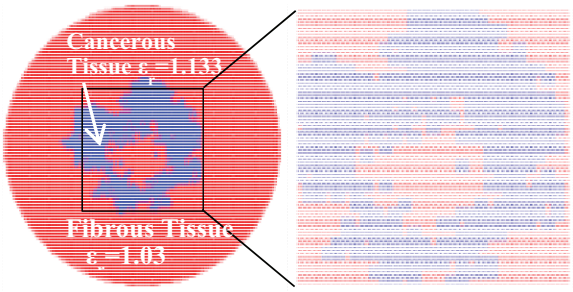


Fig. 5. 2D dipole discretization of necrotic breast cancer tumor type using $N$ = 12281 dipoles, tumor size ~1.5mm. Dipole size $d$ = 0.04 λ = 12 μm.

In all cases in this section, the tumor is discretized into $N = 12281$ dipoles with tumor size ~1.5 mm, and the dipole size is $d = 0.04\ \lambda = 12\ \mu m$ with an infinitesimal gap between dipoles (i.e., distance from center to center between each two dipoles is also $d$). The viability of tomography algorithms in imaging cancer tumor patterns is investigated through several different cancer tissue orientations. In the first example of Fig. 6, the goal is to show whether the algorithm could properly reconstruct the permittivity of cancerous tissue at the middle or the edge of tumor tissue (i.e., for negative and close to positive margins). The results show good reconstruction of cancerous tissue in both cases in Fig. 6. These simulations did not account for any noise.

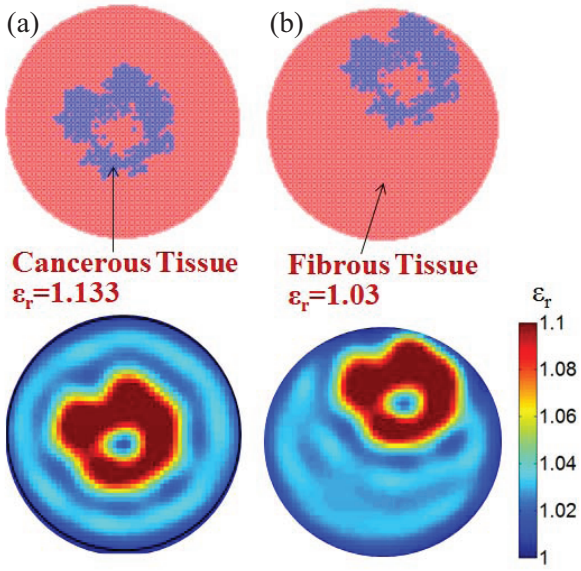


Fig. 6. Discretized DDSCAT comedo tumor (top) and reconstructed permittivity (bottom) of (a) a cancerous region with a negative margin and (b) a positive margin.

The case of Fig. 6 is repeated including random noise added to the data, up to SNR of 0 dB. The obtained images showed insignificant difference with Fig. 6 (not presented here). Figure 7 represents a similar case to Fig. 6 but for the papillary tumor pattern. The same relative permittivities of Fig. 6 are used in this case. The results show good image reconstruction as well. In order to determine the algorithm's ability to distinguish heterogeneous regions of fibrous or other normal tissue, the example of Fig. 8 is shown. In this case the permittivity of the cancerous tissue and primary background tissue are the same as in Fig. 6, but a secondary region of fibrous tissue with $\varepsilon_r = 1.08$ is used in the model. The results show successful reconstruction of the permittivity of all three tissue regions.

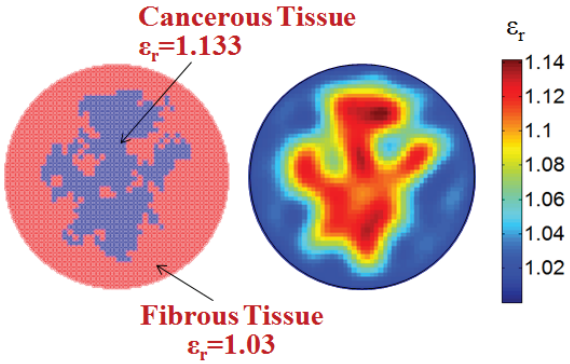


Fig. 7. Discretized DDSCAT papillary tumor (left) and reconstructed permittivity (right).

As a final demonstration of the algorithm to show the limitations of Rytov approximation in the application of the THz band, the same setup found in Fig. 8 is repeated with permittivity values corresponding to the actual electrical properties of the modeled tissues at 1 THz [4]. Note that the purpose of this setup is simply to show the need for alternative techniques for determining the shape and properties of the cancerous region when the actual permittivities of the breast tissues are used. For this setup, the tissue types are reclassified into adipose or fat tissue with $\varepsilon_r = 2.5$, fibrous tissue with $\varepsilon_r = 3.6$, and cancerous tissue with $\varepsilon_r = 4.0$. As Fig. 9 shows, the resulting reconstruction of the permittivity is not viable due to the low contrast limitation of the approximation. The reconstructed image in Fig. 9 is clearly severely degraded.

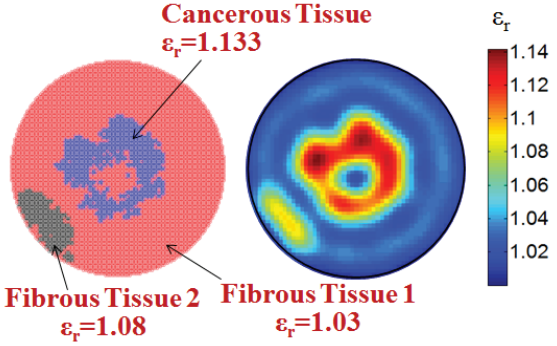


Fig. 8. Discretized DDSCAT tumor model (left) and reconstructed permittivity (right) of heterogeneous background tissue.

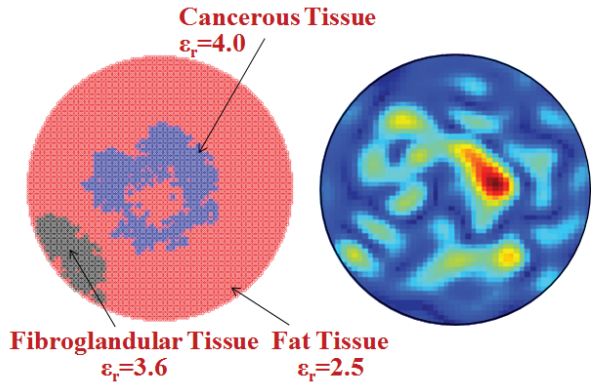


Fig. 9. Larger contrast heterogeneous tumor model (left) and reconstructed permittivity (right).

## IV. CONCLUSION AND FUTURE RESEAECH

The obtained results demonstrated imaging breast cancer margins using the linearized Rytov approximation at 1 THz. The scattered fields were calculated using the open source DDSCAT at multiple receivers created by multiple incident waves. The DDSCAT was shown to successfully model the scattered electric fields from heterogeneous and irregular tumor patterns. The reconstructed images at 1 THz demonstrate that terahertz technology has potential for the use of tumor margin assessment. However, the Rytov approximation was not particularly effective in moving toward the experimental application due to its low contrast limitation and insufficient resolution. Therefore improved imaging methods are necessary for investigating the use of THz in this application.

Ongoing research involves the use of a new nonlinear inverse scattering tomography algorithm such as the linear sample method (LSM) [25]. The Authors believe that the LSM would be able to greatly increase the resolution of the image reconstruction of breast cancer margins regardless of the contrast between cancerous and normal tissues. The use of a linear technique provides the advantage of rapid assessment of results at relatively low computational cost. It has also been shown that the LSM is not subject to the low permittivity limitations imposed on the Born approximation when utilized to determine the contrast of scatterers against the background [26]. In addition, ongoing research is focusing on measuring THz fields reflected from ex-vivo breast cancer samples in order to test the new tomography algorithm on experimental data.

## APPENDIX A

In DDSCAT, at position $j$ the dipole moment is related to the electric field as $\overline{P}_j = \alpha_j \overline{E}_{ext,j}$ where $\alpha_j$ is the polarizability tensor and $\overline{E}_{ext,j}$ is the total electric field at dipole $j$ due to both the excitation of incident waves and the interactions with the other $N$-1 dipoles. The electric field at position $j$ due to the dipole position $k$ is given by [10-14],

$$\overline{A}_{jk}\overline{P}_k = \frac{\exp(ikr_{jk})}{r_{jk}^3}\begin{bmatrix} k^2\overline{r}_{jk}\times\left(\overline{r}_{jk}\times\overline{P}_k\right)+ \\ \frac{1-ikr_{jk}}{r_{jk}^2}\times \\ \left(r_{jk}^2\overline{P}_k - 3\overline{r}_{jk}\left(\overline{r}_{jk}\cdot\overline{P}_k\right)\right)\end{bmatrix}, \quad \text{(A1)}$$

where $i=\sqrt{-1}$ and $\overline{r}_{jk}$ is the position vector between dipole $j$ and dipole $k$. Thus the complex dipole moment can be expressed as,

$$\overline{P}_j = \alpha_j\left(\overline{E}_{inc,j} - \sum_{k\neq j}^{N}\overline{A}_{jk}\overline{P}_k\right), \quad \text{(A2)}$$

which can be arranged in the matrix format,

$$\sum_{k=1}^{N}\overline{A}_{jk}\overline{P}_k = \overline{E}_{inc,j}\ . \quad \text{(A3)}$$

Equation (A3) requires solving a linear system of equations of order $3N\times3N$. The factor 3 is due to the vector position nature of the system solution at $x$, $y$, and $z$. For simplicity and reduced CPU time, the target sample is modeled as infinitely periodic targets (2D) with no variation in the $z$-direction as shown in Fig. 4. Once the complex dipole moment is obtained, the electric fields can be calculated at any point as follows [9-13],

$$\overline{E}(\overline{r}) = \sum_j\sum_{m,n}\left(\begin{array}{l}\dfrac{\exp\left(jk_0R_{jmn}\right)}{\left|R_{jmn}\right|^3}\varphi\left(R_{jmn}\right) \\ \left\{\begin{array}{l} k_0^2\overline{R}_{jmn}\times\left(\overline{P}_{jmn}\times\overline{R}_{jmn}\right)+ \\ \dfrac{\left(1-jk_0R_{jmn}\right)}{R_{jmn}^2}\left[\begin{array}{l}3\overline{R}_{jmn}\left(\overline{R}_{jmn}\cdot\overline{P}_{jmn}\right) \\ -R_{jmn}^2\overline{P}_{jmn}\end{array}\right]\end{array}\right\}\end{array}\right), \quad \text{(A4)}$$

where $\overline{R}_{jmn} = \overline{r} - \overline{r}_{jmn}$, $\overline{r}$ is the position vector of the field point and $\overline{r}_{jmn}$ is the position vector of dipole *jmn.* The vector $\overline{P}_{jmn}$ represents the polarization of dipole *jmn* and $\phi(R_{jmn})$ is a smoothing factor added to reduce the contributions from distant dipoles. In this dipole numbering, *j* represents dipoles in the unit cell, *m* and *n* represent the replica dipoles when 2D periodic boundary conditions are implemented as adopted in this work and is shown in Fig. 4.

## ACKNOWLEDGMENT

This work was sponsored by the Army Research Laboratory and was accomplished under Cooperative Agreement Number W911NF-10-2-0093. The views and conclusions contained in this document are those of the authors and should not be interpreted as representing the official policies, either expressed or implied, of the Army Research Laboratory or the U.S. Government. The U.S. Government is authorized to reproduce and distribute reprints for Government purposes not withstanding any copyright notation herein.

This work was supported in part by the National Science Foundation under Grants ARI # 0963249, MRI #0959124 (Razor), EPS #0918970 (CI TRAIN), and a grant from the Arkansas Science and Technology Authority, managed by the Arkansas High Performance Computing Center.

Funding for purchase and maintenance of the Pulsed Terahertz System is provided by NSF/MRI award #1228958. This work was supported by the NSF GRFP, the NSF GK12 Program as part of award #1228958, the Arkansas Biosciences Institute (ABI), and the Arkansas Breast Cancer Research Program (ABCRP).

## REFERENCES

[1] L. Jacobs, "Positive margins: The challenge continues for breast surgeons," *Ann. Surg. Oncol.*, vol. 15, no. 5, pp. 1271-1272, May 2008.

[2] J. Brown, T. Bydlon, L. Richards, B. Yu, S. Kennedy, J. Geradts, L. Wilke, M. Junker, J. Gallagher, W. Barry, and N. Ramanujam, "Optical assessment of tumor resection margins in the breast," *IEEE Journal of Selected Topics in Quantum Electronics*, vol. 16, no. 3, pp. 530-544, 2010.

[3] P. Ashworth, E. Pickwell-MacPherson, E. Provenzano, S. Pinder, A. Purushotham, M. Pepper, and V. Wallace, "Terahertz pulsed spectroscopy of freshly excised human breast cancer," *Opt. Express*., vol. 17, no. 15, pp. 12444-54, 2009.

[4] A. Fitzgerald, V. Wallace, M. Jimenez-Linan, L. Bobrow, R. Pye. A Purushotham, and D. Amone, "Terahertz pulsed imaging of human breast tumors," *Radiology*, vol. 239, no. 2, pp. 533-540, 2006.

[5] M. Brun, F. Formanek, A. Yasuda, M. Sekine, N. Ando, and Y. Eishii, "Terahertz imaging applied to cancer diagnosis," *Phys. Med. Biol.*, vol. 55, pp. 4615-4623, 2010.

[6] C. Ruiz and J. Simpson, "Cepstral analysis of photonic nanojet-illuminated biological cells," *Applied Computational Electromagnetics Society (ACES) Journal*, vol. 27, no. 3, pp. 215-222, March 2012.

[7] A. Hassan, D. Hufnagle, M. El-Shenawee, and G. Pacey, "Terahertz imaging for margin assessment of breast cancer tumors," *Proceedings of 2012 IEEE MTT-S International Microwave Symposium Digest*, June 2012.

[8] A. Hassan, D. Hufnagle, G. Pacey, and M. El-Shenawee, "Terahertz tomography technique for the assessment of breast cancer tumor margins," *Proceedings of 2012 IEEE Antennas and Propagation Society International Symposium*, Chicago, Illinois, July 2012.

[9] T. Bowman, A. Hassan, and M. El-Shenawee, "Terahertz frequency Born and Rytov tomography for breast cancer tumor margins," *2012 ABI Fall Research Symposium*, University of Arkansas, 23 October 2012.

[10] B. Draine and P. Flatau, "Discrete dipole approximation for scattering calculations," *J. Opt. Soc. Am. A*, vol. 11, pp. 1491-1499, 1994.

[11] B. Draine, "The discrete dipole approximation and its application to interstellar graphite grains," *J. Astrophys*., vol. 333, pp. 848-872, 1998.

[12] B. Draine and P. Flatau, "Discrete-dipole approximation for periodic targets: theory and tests," *J. Opt. Soc. Am. A*, vol. 25, pp. 2593-2703, 2008.

[13] P. Flatau and B. Draine, "Fast near-field calculations in the discrete dipole approximation for regular rectilinear grids," *Optics Express*, vol. 20, pp. 1247-1252, 2012.

[14] B. Draine and P. Flatau, "User guide to the discrete dipole approximation code DDSCAT 7.1," http://arxiv.org/abs/1002.1505v1, 2010.

[15] W. Chew, *Waves and Fields in Inhomogeneous Media*, Chapter 9, pp. 511-570, *IEEE Press*, 1995.

[16] W. Chew, "Imaging and inverse problems in electromagnetics," *Advances in Computational Electrodynamics: The Finite-Difference Time-Domain Method*, ch. 12, A. Taflove, Ed. Norwood, MA: Artech House, 1998.

[17] A. Vouldis, C. Kechribaris, T. Maniatis, K. Nikita, and N. Uzunoglu, "Investigating the enhancement of three-dimensional diffraction tomography by using multiple illumination planes," *Journal of Optical Society of America*, vol. 22, no. 7, pp. 1251-1262, July 2005.

[18] G. Dunlop, W. Boerner, and R. Bates, "On an extended Rytov approximation and its comparison with the Born approximation," *Proc. of Antennas and Propagation Society International Symposium*, vol. 14, pp 587-591, Oct. 1976.

[19] A. Vouldis, C. Kechribaris, T. Maniatis, K. Nikita, and N. Uzunoglu, "Three-dimensional diffraction tomography using filtered back propagation and multiple illumination planes," *IEEE Transactions on Instrumentation and Measurement*, vol. 55, no. 6, pp. 1975-1984, Dec. 2006.

[20] S. Ferreira Jr., M. Martins, and M. Vilela, "Reaction-diffusion model for the growth of avascular tumor," *Physical Review E*, vol. 65, no. 2, pp. 021907-1 021907-8, 2002.

[21] A. Hassan and M. El-Shenawee, "Biopotential signals of breast cancer versus tumor types and proliferation stages," *Physical Review E*, vol. 85, no. 2, pp. 021913, 2012.

[22] J. Parsons, C. Burrows, J. Sambles, and W. Barnes, "A comparison of techniques used to simulate the scattering of electromagnetic radiation by metallic nanostructures," *Journal of Modern Optics*, vol. 57, no. 5, pp. 356-365, 2010.

[23] R. Dahlbäck, T. Rubæk, M. Persson, and J. Stake, "A system for THz imaging of low-contrast targets using the Born approximation," *IEEE Transactions on THz Science and Technology*, vol. 2, no. 3, pp. 361-370, 2012.

[24] M. Hajihashemi, *Inverse Scattering Level Set Algorithm for Retrieving the Shape and Location of Multiple Targets*, Ph.D. dissertation, University of Arkansas, Fayetteville, AR, 2010.

[25] L. Crocco, I. Catapano, L. Donato, and T. Isernia, "The linear sampling method as a way to quantitative inverse scattering," *IEEE Trans. Antenn. Propag.* vol. 60, no. 4, April 2012.

[26] I. Catapano, L. Crocco, L. Donato, and T. Isernia, "Advances in inverse scattering arising from the physical meaning of the linear sampling method," *Proc. of IEEE 6th European Conference on Antennas and Propogation (EUCAP)*, pp. 3210-3214, 2001.